Influence of reduced carbon emissions and oxidation on the distribution of atmospheric CO_2: Implications for inversion analyses

Parvadha Suntharalingam,[1] James T. Randerson,[2] Nir Krakauer,[3] Jennifer A. Logan,[1] and Daniel J. Jacob[1]

[1] Recent inverse analyses constraining carbon fluxes using atmospheric CO_2 observations have assumed that the CO_2 source from atmospheric oxidation of reduced carbon is released at the surface rather than distributed globally in the atmosphere. This produces a bias in the estimates of surface fluxes. We used a three-dimensional (3D) atmospheric chemistry model (GEOS-CHEM) to evaluate the magnitude of this effect on modeled concentrations and flux estimates. We find that resolving the 3D structure of the atmospheric CO_2 source, as opposed to emitting this reduced carbon as CO_2 at the surface, yields a decrease in the modeled annual mean interhemispheric gradient (N-S) of 0.21 ppm. Larger adjustments (up to -0.6 ppm) are apparent on a regional basis in and downwind of regions of high reduced carbon emissions. We used TransCom3 annual mean simulations from three transport models to evaluate the implications for inversion estimates. The main impacts are systematic decreases in estimates of northern continental land uptake (i.e., by 0.22 to 0.26 Pg C yr^{-1}), and reductions in tropical land carbon efflux with smaller changes over oceans and in the Southern Hemisphere. These adjustments represent a systematic bias in flux estimates, accounting for changes of 9 to 27% in the estimated northern land CO_2 sink for the three models evaluated here. Our results highlight the need for a realistic description of reduced carbon emission and oxidation processes in deriving inversion estimates of CO_2 surface fluxes.

1. Introduction

[2] Top-down estimates of regional CO_2 fluxes are commonly derived from inversions of atmospheric CO_2 concentrations. A robust result of these studies over the past 15 years has been the inference of a substantial Northern Hemisphere (NH) land carbon sink [*Tans et al.*, 1990; *Enting et al.*, 1995; *Fan et al.*, 1998; *Rayner et al.*, 1999; *Bousquet et al.*, 1999; *Gurney et al.*, 2002, 2003]. These analyses, often using Bayesian methods, incorporate information on prior fluxes representing surface to atmosphere CO_2 exchange from fossil fuel combustion, oceanic uptake and the seasonal annually balanced terrestrial biosphere. The inversion procedure, constrained by observations of atmospheric CO_2, then estimates "residual" surface CO_2 fluxes that account for additional influences such as biomass burning, deforestation and regrowth, CO_2 and nutrient fertilization, and interannual climate variability as well as for errors in the prior flux distributions.

[3] Recent inverse analyses have not explicitly resolved the tropospheric source of CO_2 from oxidation of reduced carbon species (CO, CH_4, and non-methane volatile organic compounds (NMVOCs)), although this source has been accounted for in past studies [*Enting and Mansbridge*, 1991; *Enting et al.*, 1995]. Instead, as detailed below, this constituent carbon is actually included in the prior inventories employed in these analyses, where it is represented as surface emission of CO_2. The long tropospheric lifetimes of methane and carbon monoxide (8–12 years and 1–4 months, respectively) [*Crutzen*, 1994; *Prather*, 1996] result in these reduced carbon species being transported on a global scale far from their surface release location before being oxidized to CO_2; specifically, the distributions of CH_4 and CO oxidation are primarily governed by the abundance of OH radicals, and thus peak in the tropics [*Spivakovsky et al.*, 2000]. There is, therefore, a systematic discrepancy between the actual distribution of the CO_2 source from reduced carbon oxidation and the modeled representation (that assumes surface emissions of CO_2) employed in many inverse analyses. The observations

[1]Division of Engineering and Applied Sciences, Harvard University, Cambridge, Massachusetts, USA.
[2]Department of Earth System Science, University of California, Irvine, California, USA.
[3]Division of Geological and Planetary Sciences, California Institute of Technology, Pasadena, California, USA.

used to constrain the inversion capture the actual processes of emissions and tropospheric oxidation, whereas the models do not. Neglecting the three-dimensional (3D) representation of these processes in modeled CO_2 fields will, thus, introduce a bias in the "observed minus modeled" concentration residuals constraining the inversion, and hence also in the estimates of surface fluxes. In this study we explore the role of this atmospheric "chemical pump" which represents the transport of reduced carbon trace gases from the surface to remote locations prior to their oxidation to CO_2. We also evaluate the impact of accounting for it in atmospheric CO_2 inversions. Specifically, we (1) assess the magnitude of the bias in modeled CO_2 concentrations caused by neglecting the emissions and oxidation of reduced trace gases, and (2) evaluate its impact on inversion flux estimates.

[4] Estimates of global emissions of CO, CH_4, and NMVOCs are 0.5, 0.4, and 0.6 Pg C yr^{-1} respectively [*Intergovernmental Panel on Climate Change (IPCC)*, 2001; *World Meteorological Organization (WMO)*, 1999]. Tropospheric oxidation of these species (primarily by the hydroxyl radical OH) provides a CO_2 source of 0.9–1.3 Pg C yr^{-1} (B. N. Duncan et al., Model study of the variability and trends of carbon monoxide (1988–1997): Model formulation, evaluation and sensitivity, manuscript in preparation, 2005) (hereinafter referred to as Duncan et al., manuscript in preparation, 2005), as almost all the CH_4 and a significant portion of the NMVOCs are oxidized to CO and subsequently to CO_2 [*Logan et al.*, 1981; *Altshuller*, 1991]. This source is comparable in magnitude to estimates of annual mean ocean and land biosphere CO_2 sinks [*IPCC*, 2001].

[5] Recent inverse analyses account for this source as surface CO_2 emissions in prior inventories. The $1° \times 1°$ distribution of *Andres et al.* [1996] of annual mean CO_2 emissions from fossil fuel and cement manufacture, for example, is based on the methodology of *Marland and Rotty* [1984] and *Marland et al.* [1985]. These estimates derive CO_2 emissions assuming complete combustion of the carbon fraction oxidized in each fuel type. This methodology is employed for annual inventories under the following assumptions: (1) Oxidation to CO_2 of many reduced carbon combustion products will be complete within the span of a year given their relatively short tropospheric lifetimes (e.g., a few months for CO, hours to days for many non-methane hydrocarbons); and (2) oxidation of reduced carbon compounds with lifetimes longer than 1 year (e.g., CH_4) can be accounted for by assuming that production rates and fraction oxidized are invariant from year to year [*Marland and Rotty*, 1984].

[6] For recent inversions, prior fluxes accounting for the annually balanced terrestrial biospheric seasonal cycle have been modeled as a balance between CO_2 fluxes representing photosynthetic uptake and total ecosystem respiration loss [*Denning et al.*, 1995; *Rayner et al.*, 1999; *Bousquet et al.*, 1999; *Gurney et al.*, 2002]. However, as *Randerson et al.* [2002] note, the definition of a regional NEP (Net Ecosystem Production), representing the mass rate of change of carbon within the terrestrial biosphere must inherently include non-respiratory carbon losses from the biosphere. They estimate that non-respiratory carbon losses, including methane and NMVOCs, fires, leaching of soil organic carbon and river fluxes account for ~5 Pg C yr^{-1} (~10% of global net primary production (NPP)). The priors, consisting of seasonally varying terrestrial carbon exchange (e.g., CASA [*Potter et al.*, 1993; *Randerson et al.*, 1997] and the Simple Biosphere land surface model (SiB) [*Sellers et al.*, 1996; *Denning et al.*, 1996]), have typically accounted for the reduced carbon component of this flux from the biosphere by representing it as surface emission of CO_2; that is, the reduced carbon flux is implicitly subsumed in these prior distributions.

[7] The impact of non-CO_2 carbon fluxes from the biosphere via leaching and rivers on atmospheric CO_2 concentrations has been investigated elsewhere and will not be addressed here. *Sarmiento and Sundquist* [1992] calculated a pre-industrial ocean to atmosphere flux of 0.6 Pg C yr^{-1} originating from riverine carbon. Using ocean and atmospheric transport models, *Aumont et al.* [2001] estimated the contribution of this carbon source to the atmospheric gradient (North Pole-South Pole) to be −0.6 ppm, as a result of land to ocean river carbon fluxes in the NH and subsequent outgassing of CO_2 from the Southern Ocean.

[8] *Enting* [2002] highlights the importance of distinguishing between CO_2 and carbon fluxes when constructing atmospheric CO_2 simulations for inverse analyses. The impact of reduced carbon oxidation on CO_2 inversions has previously been addressed by *Enting and Mansbridge* [1991] and *Enting et al.* [1995], who accounted for a tropospheric CO_2 source from CO oxidation, and also removed this carbon from prior surface inventories, in annual mean inversions with a global 2D (zonally averaged) transport model. The tropospheric CO_2 source from CO oxidation in these analyses was taken to be 0.86 Pg C yr^{-1} and had an annual mean, zonally averaged and uniform vertical distribution (i.e., the only variation in the source distribution was latitudinal). Their reduced carbon budget accounted for annual mean zonally averaged sources from fossil fuel combustion and the biosphere, and for CO loss to soils. More recently, *Baker* [2001] presented results from a 3D atmospheric CO_2 inversion that included an annual mean tropospheric source of CO_2 from CO oxidation. This analysis did not remove the reduced carbon source from prior surface inventories and thus accounted only for a portion of the chemical pump bias.

[9] Our work extends these previous studies by accounting for (1) seasonally varying biospheric reduced carbon sources (including biogenic NMVOC emissions), and (2) improved representation of the seasonal and spatial structure of the 3D reduced carbon source of CO_2. We conduct our analysis using a 3D chemical transport model (GEOS-CHEM) and employed the most recent estimates of reduced carbon fluxes from combustion and biospheric sources (see Table 1). We also place our results in the context of recent atmospheric inversions (e.g., TransCom3 [*Gurney et al.*, 2002, 2003]) using *GLOBALVIEW-CO₂*

Table 1. Global Atmospheric Production of CO$_2$ From Reduced Carbon Oxidation

Reduced Carbon Source	Contribution to CO$_2$ in Standard Simulation,[a] Pg C yr^{-1}
CO total	0.50
Fossil	0.20
Biofuels	0.08
Biomass burning	0.21
CH$_4$ total[b]	0.39
Energy	0.07
Biomass burning	0.016
Other biosphere	
Wetlands	0.14
Ruminants	0.062
Rice	0.044
Termites	0.019
Landfills	0.039
NMVOCs total[c]	0.22
Energy	0.03
Biomass burning	0.03
Biosphere	0.16
Total	**1.1**

[a]Reduced carbon emissions estimates are taken from Duncan et al. (manuscript in preparation, 2005) and *Wang et al.* [2004]. We assume a CO$_2$ yield of 1 from CH$_4$ and CO oxidation. The CO$_2$ yield from NMVOC oxidation represents the component via CO and is a weighted average of the CO yields from Duncan et al. (manuscript in preparation, 2005) (see their Table 9). In the standard simulation the combustion sources for CO and CH$_4$ and NMVOC emission have spatial distributions taken from Duncan et al. (manuscript in preparation, 2005) (fossil fuel), *Yevich and Logan* [2003] (biofuels) and *Duncan et al.* [2003] (biomass burning). CO production from biogenic NMVOC oxidation follows the distribution of Duncan et al. (manuscript in preparation, 2005), which is based on work by *Guenther et al.* [1995] (for isoprene, monoterpenes and methanol) and *Jacob et al.* [2002] (for acetone). Other CH$_4$ sources are distributed according to the a priori distributions of *Wang et al.* [2004] as follows: *Walter et al.* [2001] (wetlands); EDGAR v3.2 [*Olivier*, 2002] (ruminants, rice, landfills); *Sanderson* [1996] (termites).

[b]The methane sources in the "Energy" category are from petroleum, coal combustion and natural gas.

[c]The NMVOC sources in the "Energy" category are from fossil and domestic fuel combustion. NMVOC sources in the "Biosphere" category are carbon emissions from vegetation, primarily isoprene, terpenes and acetone.

[2003] observations, and examine the implications for regional flux estimates.

2. Calculation of the Chemical Pump Effect

[10] Most atmospheric CO$_2$ inversion studies optimize estimates of surface fluxes by minimizing the sum of a squared difference between observed and modeled CO$_2$ concentrations and a penalty term proportional to the squared difference between the estimated surface fluxes and their prior magnitudes [*Enting et al.*, 1995; *Bousquet et al.*, 1999; *Peylin et al.*, 2002; *Gurney et al.*, 2002]. The cost function generally takes the form [*Enting*, 2002],

$$J(\mathbf{x}) = (\mathbf{Hx} - \mathbf{y_0})^{\mathrm{T}}\mathbf{R_0}^{-1}(\mathbf{Hx} - \mathbf{y_0}) + (\mathbf{x} - \mathbf{x_b})^{\mathrm{T}}\mathbf{S_0}^{-1}(\mathbf{x} - \mathbf{x_b}). \tag{1}$$

Here $\mathbf{x}$ represents a vector of surface fluxes to be estimated and $\mathbf{x_b}$ represents the a priori values. $\mathbf{Hx}$ and $\mathbf{y_0}$ are, respectively, the modeled and observed CO$_2$ concentrations, where $\mathbf{H}$ represents the linearized model transport matrix. $\mathbf{R_0}$ and $\mathbf{S_0}$ are covariance matrices accounting for errors in the

representation of modeled and observed concentrations and in the a priori fluxes respectively.

[11] We calculate the effect of the chemical pump on modeled CO$_2$ concentrations ("the chemical pump concentration adjustment") with a 3D atmospheric chemistry model (GEOS-CHEM), to account for (1) the inclusion of the tropospheric CO$_2$ source from reduced carbon oxidation (concentration increase, $+\mathbf{\Delta y_{ox}}$) and (2) the removal of the reduced carbon from surface CO$_2$ emission inventories (concentration decrease $-\mathbf{\Delta y_{surf}}$). Omission of the proper representation of both these effects (points 1 and 2) will give rise to two separate sources of error in atmospheric inverse analyses.

[12] We then define a chemical pump adjustment ($\mathbf{\Delta y}$) to the modeled CO$_2$ concentration ($\mathbf{Hx}$) as

$$\mathbf{\Delta y} = +\mathbf{\Delta y_{ox}} - \mathbf{\Delta y_{surf}}. \tag{2}$$

The chemical pump adjustment thus quantifies the effect on modeled concentrations of properly accounting for the emission, transport and oxidation of reduced carbon species, as opposed to emitting the same CO$_2$ from surface inventories. In an inversion that focuses solely on CO$_2$ (and neglects the 3D representation of the reduced carbon contribution), $\mathbf{\Delta y}$ is the quantity that should be added to the modeled concentration term ($\mathbf{Hx}$) before the minimization of equation (1).

[13] To calculate $\mathbf{\Delta y}$ we conduct two global CO$_2$ simulations, each determining one of the terms on the right-hand side of equation (2). The first simulation (simulation "CO2-3D" to obtain $\mathbf{\Delta y_{ox}}$) represents the impact of the 3D CO$_2$ source from reduced carbon oxidation. We obtain this distribution using the GEOS-CHEM model as detailed further below. The second simulation (simulation "CO2-SURF" to obtain $\mathbf{\Delta y_{surf}}$) represents the effect of emitting this carbon as CO$_2$ in surface emission inventories for fossil and biospheric emissions. The distribution for this source is calculated as a composite one that accounts for all the surface emissions patterns of the reduced carbon species and processes listed in Table 1. The global CO$_2$ source from reduced carbon species is the same in both "CO2-3D" and "CO2-SURF" simulations (1.1 Pg C yr^{-1}, Table 1); the only difference is the distribution pattern. We calculate the distribution of the chemical pump adjustment, $\mathbf{\Delta y}$, as the concentration difference between CO2-3D and CO2-SURF (equation (2)).

[14] Both simulations are driven by monthly mean source fields. They are spun up from a constant initial condition (370 ppm) for four years (the time span recommended by the TransCom Level 1 protocol to allow inter-hemispheric gradients to stabilize [*Gurney et al.*, 2002]), driven by repeated meteorological data for 2001. We report the results of the fourth simulation year.

[15] The GEOS-CHEM model (version 5.07) is driven by assimilated meteorological observations from the Goddard Earth Observation System (GEOS) of the NASA Global Modeling and Assimilation Office (GMAO) [*Bey et al.*, 2001]. The resolution is 2° × 2.5° in the horizontal, there are 30 vertical sigma levels, and the dynamic time step is 15 min. Previous application of GEOS-CHEM to simulation of CO$_2$ is described by *Suntharalingam et al.* [2004].
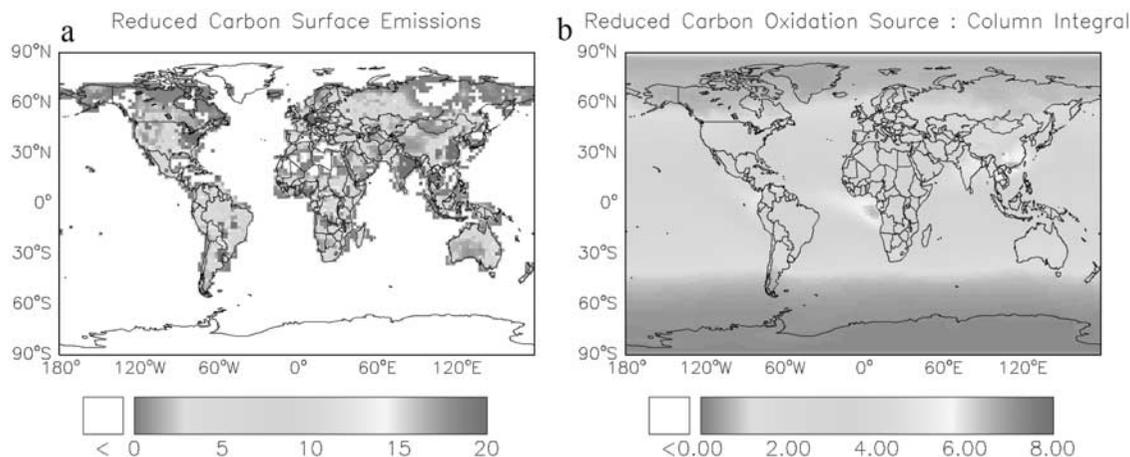
Figure 1. Global distributions of the CO_2 source from (a) surface emissions of these reduced carbon trace gases (the fluxes specified in the CO2-SURF simulation, left panel); and (b) the oxidation of reduced carbon trace gases (the column integrals of the CO_2 fluxes from the CO2-3D simulation, right panel). The total carbon source is the same in both distributions (1.1 $PgCyr^{-1}$). Units are $gC\ m^{-2}\ yr^{-1}$. The two panels have different color scales to highlight spatial features. See color version of this figure at back of this issue.

[16] We now discuss in detail, the derivation of simulation CO2-3D. Calculating the oxidation source of CO_2 (Δy_{ox}) requires accounting for the transport, oxidation, and CO_2 yields of methane, NMVOCs, and CO. We use for this purpose the GEOS-CHEM CO simulation of Duncan et al. (manuscript in preparation, 2005), which accounts for direct emissions of CO as well as for atmospheric production of CO from oxidation of methane and NMVOCs (Table 1). The methane oxidation source in that simulation is computed by applying monthly mean 3D OH concentration fields to latitudinally dependent methane concentrations from NOAA/CMDL observations (averaged over 1988–1997), with a CO yield of unity. The NMVOC oxidation source is treated as an equivalent CO emission on the basis of NMVOC emission inventories and species-specific CO yields ranging from 0.2 to unity [*Altshuller*, 1991]. The loss of CO from oxidation by OH is computed using the previously mentioned global 3D OH fields, and defines our chemical source of CO_2 (simulation CO2-3D) with global magnitude of 1.1 Pg C yr^{-1} (Table 1). Duncan et al. (manuscript in preparation, 2005) evaluated their CO simulation extensively with observations from surface sites and aircraft and showed that the simulation has no significant global bias and provides a realistic global 3D CO concentration field.

[17] The above approach assumes that atmospheric production of CO_2 from oxidation of methane and NMVOCs necessarily involves CO as an intermediate. The main recognized oxidation pathway bypassing CO to form CO_2 is the reaction of peroxyacyl radicals (RCO_3) with NO, and is estimated to amount to less than 0.05 Pg C yr^{-1} according to current global atmospheric chemistry models (A. Fiore, personal communication, 2004). This is small relative to the 1.1 Pg C yr^{-1} source of CO_2 from CO oxidation.

[18] The CO2-SURF simulation represents the effect of emitting the reduced carbon sources, as a CO_2 equivalent, from the surface inventories given in Table 1 and consistent with the Duncan et al. (manuscript in preparation, 2005)

simulation. The methane source is distributed according to the a priori methane inventory of *Wang et al.* [2004]. Table 1 gives details of the magnitudes and global distribution patterns employed for emission of all reduced carbon species in the CO2-SURF simulation.

3. Impact of Chemical Pump on Atmospheric CO_2 Distributions

[19] Figure 1 compares the spatial distributions of the annual CO_2 source in the CO2-3D and CO2-SURF simulations. Figure 1a represents the column-integral of CO_2 production from CO oxidation for the CO2-3D simulation. Figure 1b shows the distribution of surface emissions of reduced carbon species from fossil fuel combustion, biomass burning, and biospheric processes listed in Table 1 and underlying simulation CO2-SURF. Figure 2 presents the comparison on a zonally integrated basis as a function of latitude. The CO2-3D source shows a diffuse pattern peaking in the tropics, while the CO2-SURF source is confined to the populated continents and shows a northern hemispheric displacement relative to the 3D reduced carbon oxidation source. The CO2-SURF distribution is highly localized and influenced by regions of high fossil and biofuel CO emissions in east Asia and northern India, biomass burning CO in tropical Africa and south America, and fossil fuel and biogenic CO in the eastern United States [*Duncan et al.*, 2003; *Yevich and Logan*, 2003, Duncan et al., manuscript in preparation, 2005]. The vertical distribution of the 3D CO_2 source from reduced carbon oxidation peaks in the tropics at an altitude of 3–4 km, primarily reflecting the distribution of OH radicals [*Spivakovsky et al.*, 2000].

[20] The annually averaged surface CO_2 concentrations for the two simulations, representing Δy_{ox} and Δy_{surf}, are shown in Figure 3, and reflect the underlying source distributions. Surface concentrations are generally higher with a greater degree of localized structure for Δy_{surf} than for Δy_{ox}, as is expected, since the entire CO_2 source in
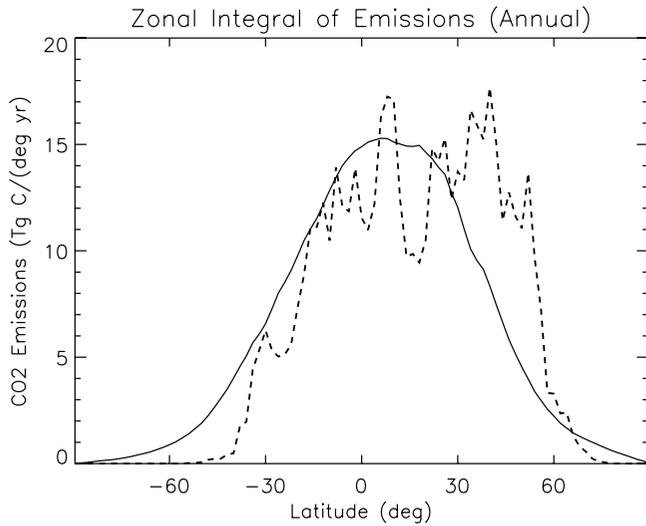
Figure 2. Zonal integrals of the chemical source of CO$_2$ computed from reduced carbon oxidation using GEOS-CHEM (CO2-3D simulation, solid line) or specified as a surface flux (CO2-SURF simulation, dashed line).

CO$_2$-SURF is confined to the surface. Δy_{surf} is highest in and downwind of regions of high reduced carbon emissions (China, northern India, Europe and the eastern United States). In contrast, Δy_{ox} is smaller, more diffuse and displays a maximum in the northern tropics. The somewhat higher NH surface values for Δy_{ox} result from its dependence on the CO2-3D source, which represents a convolution of the distribution of OH radicals and the reduced carbon mixing ratio distribution (the latter has a Northern Hemispheric bias).

[21] Figure 4 shows the spatial distribution of the annually averaged value of Δy (the chemical pump concentration adjustment) at the surface, i.e., the difference between the Δy_{ox} and Δy_{surf}. The corresponding zonally averaged

latitudinal gradient is shown in Figure 5. The chemical pump adjustment at the surface is largest in absolute value downwind of regions of high reduced carbon emissions. Δy values less than −0.3 ppm occur extensively in continental regions of eastern China, eastern Europe, northern India and the eastern United States. The mean north-south interhemispheric difference is −0.21 ppm.
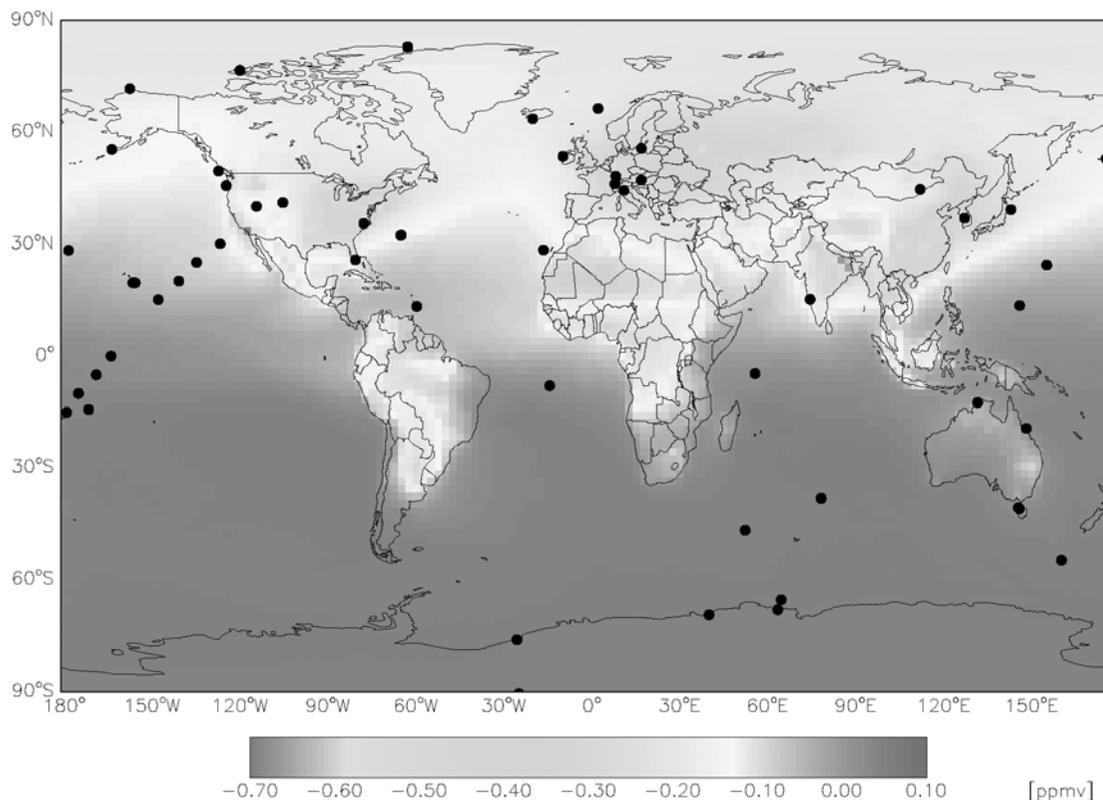
[22] In the TransCom3 inverse study of *Gurney et al.* [2002], observational constraints for regional flux estimates were provided by annual mean concentration residuals at 76 GLOBALVIEW-CO2 sites (locations shown in Figure 4). These residuals represent differences between modeled and observed concentrations, where modeled concentrations are based on prior "background" fluxes accounting for fossil fuel combustion, the seasonal terrestrial biosphere, and air-sea exchange. In Figure 6 we show the impact of the chemical pump adjustment on concentration residuals from the TransCom3 annual mean study by plotting the original residuals from *Gurney et al.* [2002] at the GLOBALVIEW-CO$_2$ sites (their Figure 2) along with the adjusted residuals using values of Δy from our analysis. The chemical pump adjustment imposes a systematic decrease on modeled concentrations at northern hemispheric sites. For this configuration of stations, the north-south inter-hemispheric difference for the annual mean value of Δy is −0.20 ppm.

[23] The interhemispheric difference of the concentration residuals (mean across all models) used to constrain the annual mean TransCom3 inversion was 2.3 ppm. This north-south difference led to a a northern continental carbon sink estimate of 2.2 Pg C yr^{-1} (mean across all models) (K. Gurney, personal communication, 2004). The chemical pump effect would decrease this interhemispheric difference of residuals by about 10%, and imply correspondingly lower northern continental carbon uptake in inverse analyses.

[24] The distribution of Δy is driven by two factors (equation (2)): (1) the addition of a tropospheric source of CO$_2$ from the transport and oxidation of reduced carbon
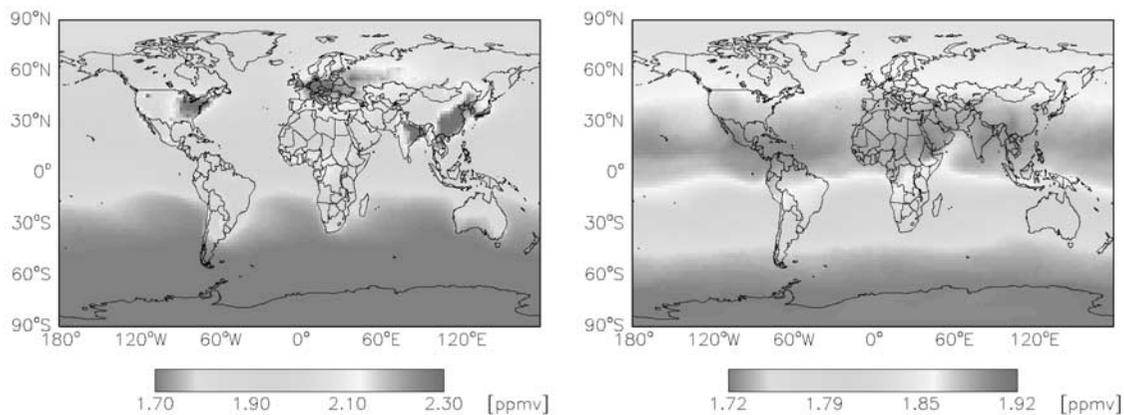
Figure 3. Surface CO$_2$ concentration distributions from (left) the CO2-SURF simulation (for Δy_{surf}) and (right) the CO2-3D simulation (for Δy_{ox}). Values shown are the annual mean concentration in the fourth simulation year, and following subtraction of the initial condition (370 ppm). The two panels have different color scales to highlight spatial features. See color version of this figure at back of this issue.

Figure 4. Spatial distribution of the chemical pump concentration adjustment $\Delta\mathbf{y}$ at the surface (annual mean). This distribution represents the difference between the left and right panels of Figure 3 ($\Delta\mathbf{y}_{ox} - \Delta\mathbf{y}_{surf}$). Units are ppm. The black circles represent the GLOBALVIEW-CO2 stations used in the inversion analysis of *Gurney et al.* [2002]. See color version of this figure at back of this issue.

trace gases ($\Delta\mathbf{y}_{ox}$) and (2) the removal of the equivalent reduced carbon source from surface inventories ($\Delta\mathbf{y}_{surf}$). The Northern Hemisphere minimum in Figure 5 can be ascribed to the dominance of $\Delta\mathbf{y}_{surf}$ over $\Delta\mathbf{y}_{ox}$ at the surface. However, Figure 4 demonstrates that it is the highly localized nature of $\Delta\mathbf{y}_{surf}$ that has the greatest impact on the surface spatial distribution. While remote ocean sites show changes of 0.1 ppm or less, the values of $\Delta\mathbf{y}$ at Northern Hemisphere continental GLOBALVIEW-CO2 sites in or downwind of regions of reduced carbon emissions are substantial: −0.56 ppm (TAP), −0.36 ppm (HUN), −0.36 ppm (ITN), and −0.29 ppm (BAL). The concentration residual differences between stations (in the longitudinal direction) used to constrain regional and continental scale flux estimates in the TransCom3 annual mean inversion were generally less than 1 ppm (K. Gurney, personal communication, 2004). Accounting for the chemical pump adjustment, therefore, is likely to play an important role in the determination of regional flux estimates.

## 4. Implications for Flux Estimates From CO_2 Inversions

[25] To evaluate the impact of the chemical pump adjustment on carbon flux estimates from atmospheric CO_2 inversions, we replicate the methodology of the TransCom3 Level 1 analysis [*Gurney et al.*, 2002,

2003]. This inversion method, constrained by concentration residuals at GLOBALVIEW-CO2 stations (Figures 4 and 6), estimates residual CO_2 fluxes for 11 land regions and 11 ocean regions.

[26] *Gurney et al.* [2002, 2003] note that model transport differences represent a significant source of uncertainty in
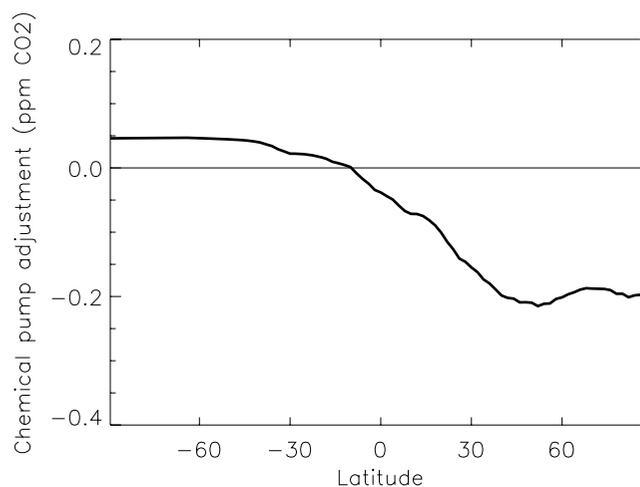
Figure 5. Zonally and annual averaged value of the chemical pump adjustment $\Delta\mathbf{y}$ at the surface.
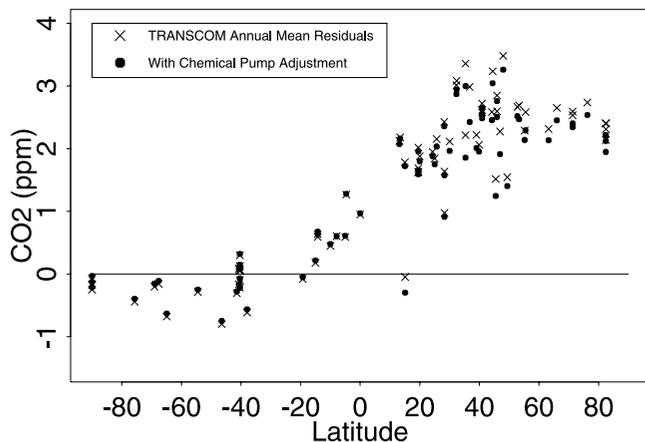
Figure 6. Impact of the chemical pump adjustment at GLOBALVIEW-CO2 sites on the mean CO_2 residuals from Figure 2 of *Gurney et al.* [2002]. These residuals represent the difference between model estimates of the interhemispheric distribution of CO_2 (caused by fossil fuels, ocean exchange, and an annually balanced terrestrial biosphere) and observations. The crosses correspond to the mean value (averaged over all models of the TransCom3 study) of the residuals at each station. The solid circles represent the effect of adjusting these residuals using the Δy value calculated in this study.

inversion flux estimates on both hemispheric and regional scales. We use here transport fields from three different models that participated in TransCom3: (1) MATCH with NCAR-CCM winds [*Krakauer et al.*, 2004; *Mahowald et al.*, 1997]; (2) LSCE-TM2 [*Heimann*, 1995; *Bousquet et al.*, 1999]; and (3) GISS-UCI (*Prather et al.*, 1987; *Hansen et al.*, 1997]. (Transport fields for the latter two models were taken from the TransCom website (http://transcom.colostate.edu/TransCom_3/transcom_3.html) where the individual model basis functions are archived.) These three models displayed characteristics spanning the TransCom3 range [*Gurney et al.*, 2003, Table 3].

[27] We derive new inversion estimates of regional residual fluxes after incorporating the chemical pump concentration adjustment into the modeled concentration fields (**Hx**). The bias in flux estimates due to neglecting the chemical pump effect is then given by the difference between the new flux estimates and the original values, and denoted "the chemical pump flux adjustment." The methodology, prior fluxes and covariance matrices used in the inversion follow the TransCom3 level 1 protocol (*Gurney et al.* [2002], with adjustments following *Krakauer et al.* [2004] (i.e., application of generalized cross validation to select uncertainty ranges of terrestrial prior flux estimates and the weighting of CO_2 station data)).

[28] *Gurney et al.* [2002] point out that fluxes integrated over latitudinal zones are better constrained by the observations than individual regional results. In Table 2 we summarize results for zonally aggregated regions. Also listed in Table 2 are the initial estimates from the models

prior to the chemical pump adjustment. The sign convention in this table is that a negative flux denotes net uptake (into the biosphere or ocean). A positive chemical pump flux adjustment (defined as the difference between the flux estimate after chemical pump adjustment minus the original flux estimate) therefore represents a decrease in the net uptake flux, or an increase in net efflux.

[29] Since the chemical pump adjustment has its primary impact on modeled concentration residuals at Northern Hemisphere sites in and downwind of continental regions of high reduced carbon emissions (Figure 6), the main effect on inversion estimates is a decrease in estimated uptake by land in most northern land regions for all three models. The TransCom3 regions of boreal and temperate Asia, North America and Europe all show systematic positive flux adjustments which represent reductions in net carbon uptake. The aggregated region of Europe and boreal and temperate Asia is most affected by the chemical pump adjustment for all three models (Table 2). Decreases in estimated flux uptake of 0.15 to 0.24 Pg C yr^{-1} are seen there, in contrast to 0.01 to 0.07 Pg C yr^{-1} for North America. The total northern extra-tropical land flux adjustment (0.22–0.27 Pg C yr^{-1}) and the total zonal integral (for northern extra-tropical ocean and land) (0.18 to 0.21 Pg C yr^{-1}) display less variability across models than do the estimates for the individual regions.

[30] The relative impact of the chemical pump flux adjustment is quite model dependent (e.g., 9% of the original northern extra-tropical uptake level in MATCH, but 27% for the LSCE-TM2 model, Table 2). This arises from model disagreement over the magnitude of the northern land sink (−2.5 ± 0.4 Pg C yr^{-1} to −0.9 ± 0.5 Pg C yr^{-1}, Table 2), and its longitudinal partition in the original inversion estimates; for example, TM2-LSCE attributes the major part of the uptake to north America, in contrast to MATCH and GISS-UCI which locate it in Europe and north Asia.

[31] The tropics are the most poorly constrained regions in the Level 1 inversion due to the small number of observing sites, resulting in large a posteriori uncertainties on flux estimates [*Gurney et al.*, 2002, 2003; *Krakauer et al.*, 2004]. Estimated flux adjustments are smaller than in the northen midlatitudes, and represent reductions in CO_2 efflux (−0.14 to −0.17 Pg C yr^{-1} for the aggregated land, Table 2). We do not address this further in view of the limited observational constraints here.

[32] Oceanic regions, where the observation sites are not as affected by the chemical pump concentration adjustment, generally display much smaller flux adjustments than for the land. Table 2 indicates that the aggregated northern extra-tropical oceans display slightly increased uptake under the chemical pump adjustment, while the tropical oceans display slightly reduced efflux (in common with tropical land).

[33] All three models ascribe very small chemical pump flux adjustments in the southern extratropics (on the order of 0.02 Pg C yr^{-1} for aggregated land and ocean areas) driven by the very small concentration adjustments here (Figure 4). Although some regions of the Southern Hemispheric continents display concentration adjustments of

Table 2. Regionally Aggregated Chemical Pump Flux Adjustments for an Annual Mean Inversion[a]

Region	MATCH Flux Estimates			LSCE Flux Estimates			GISS Flux Estimates		
	Original	Adjusted	Bias	Original	Adjusted	Bias	Original	Adjusted	Bias
North America	−0.70 ± 0.3	−0.62	**0.07**	−0.8 ± 0.4	−0.84	**0.01**	−0.29 ± 0.4	−0.25	**0.03**
Northern Asia and Europe	−1.81 ± 0.3	−1.67	**0.15**	−0.07 ± 0.5	0.17	**0.24**	−1.06 ± 0.5	−0.82	**0.24**
Northern land[b]	−2.51 ± 0.4	−2.29	**0.22**	−0.91 ± 0.5	−0.67	**0.25**	−1.35 ± 0.5	−1.08	**0.27**
Northern ocean[b]	−0.39 ± 0.3	−0.40	**−0.01**	−1.76 ± 0.4	−1.81	**−0.05**	−2.06 ± 0.5	−2.15	**−0.08**
Tropical land[b]	1.0 ± 0.7	0.86	**−0.14**	0.02 ± 0.8	−0.15	**−0.17**	0.32 ± 0.8	0.18	**−0.14**
Tropical ocean[b]	0.66 ± 0.3	0.62	**−0.04**	0.50 ± 0.2	0.48	**−0.02**	0.98 ± 0.3	0.94	**−0.03**
Southern land[b]	−0.71 ± 0.6	−0.73	**−0.02**	−0.01 ± 0.6	0.01	**0.02**	0.19 ± 0.6	0.21	**0.02**
Southern ocean[b]	−0.88 ± 0.3	−0.86	**0.02**	−0.66 ± 0.4	−0.68	**−0.03**	−0.90 ± 0.4	−0.93	**−0.03**

[a]Units are Pg C yr⁻¹.
[b]Results are shown on a regionally aggregated basis and for three transport models. Also shown for each model are the flux estimates with and without the chemical pump adjustment to model concentrations (columns 1 and 2 for each model). A posteriori uncertainties on flux estimates are given in the first column for each model. The regional totals are aggregated over the TransCom3 regions as follows: Northern land is the sum of boreal and temperate North America, boreal and temperate Asia and Europe. Tropical land is the sum of tropical America, tropical Asia and northern Africa. Southern land is the sum of South America, Southern Africa and Australia. Northern ocean is the sum of the North Pacific, the North Atlantic, and the Northern Ocean. Tropical ocean is the sum of the tropical east and west Pacific, the tropical Atlantic and the tropical Indian Ocean. Southern ocean is the sum of the south Indian ocean, the south Atlantic, the south Pacific and the Southern Ocean.

magnitude up to 0.1 ppm, the majority of the observation sites are oceanic, and register small Δy values.

5. Discussion and Conclusions

[34] Recent inverse analyses constraining carbon fluxes using atmospheric CO₂ observations assume that the CO₂ source from atmospheric oxidation of reduced carbon (1.1 Pg C yr⁻¹) is released at the surface rather than distributed globally in the atmosphere. This produces a bias in the estimates of surface fluxes. We used a 3D atmospheric chemistry model (GEOS-CHEM) to evaluate the magnitude of this "chemical pump" effect on modeled concentrations and flux estimates. We find that resolving the 3D structure of the atmospheric CO₂ source, as opposed to emitting this reduced carbon as CO₂ at the surface, yields a decrease in the modeled annual mean inter-hemispheric gradient (N-S) of 0.21 ppm. Larger adjustments (up to −0.6 ppm) are apparent on a regional basis in and downwind of regions of high emissions of reduced carbon.

[35] We used TransCom3 annual mean simulations from three transport models to evaluate the implications for inversion estimates. The main impacts are systematic decreases in estimates of northern continental land uptake (i.e., by 0.22 to 0.27 Pg C yr⁻¹), and reductions in tropical land carbon efflux (−0.14 to −0.17 Pg C yr⁻¹), with smaller changes over oceans and in the Southern Hemisphere. While these adjustments are generally smaller than the a posteriori uncertainties calculated by the inversion (e.g., 0.4 to 0.5 Pg C yr⁻¹ for northern land uptake, Table 2), they represent a systematic bias in flux estimates. They account for changes of 9 to 27% in estimated northern land CO₂ uptake for the three models evaluated here. Our results highlight the need for a realistic description of reduced carbon emission and oxidation processes in deriving inversion estimates of CO₂ surface fluxes.

[36] Our standard simulation is based on a global CO₂ source from reduced carbon oxidation of 1.1 Pg C yr⁻¹. Previous literature estimates for reduced carbon emissions [WMO, 1999; Bergamaschi et al., 2000; Kasibhatla et al., 2002; Petron et al., 2002] imply a likely range of 0.9–1.3 Pg C yr⁻¹ for this source. As a sensitivity study we

increased the fossil and biofuel source by 0.12 Pg C yr⁻¹ in our simulation, on the basis of the CO inversion results of *Petron et al.* [2002] and *Kasibhatla et al.* [2002]. The resulting chemical pump concentration adjustment gives an inter-hemispheric difference of −0.25 ppm (as measured at the surface GLOBALVIEW-CO2 sites), in contrast to −0.20 ppm in our standard simulation. Corresponding flux adjustments from the three models display similar changes on a zonally averaged basis, for example, an additional 0.07 Pg C yr⁻¹ decrease in northern extra-tropical land uptake to give a flux adjustment range of 0.29 to 0.33 Pg C yr⁻¹. This scenario illustrates that uncertainties in reduced carbon budget terms can have consequences for inverse CO₂ flux estimates disproportionate with their magnitude. Although a change of only 10% was introduced to the global reduced carbon budget, the resulting concentration and flux adjustments for Northern Hemisphere land changed by more than 25%. This resulted from the way in which reduced carbon distributions were modified in this sensitivity test; specifically, the increase in the CO budget was confined to fossil and biofuel sectors, with consequent local implications for observation sites downwind of the predominantly northern hemispheric emission regions.

[37] Variations in the OH field underlying the reduced carbon oxidation source will affect the distribution of the CO2-3D simulation. Variability in global mean OH has been estimated to be under 10% [*Spivakovsky et al.*, 2000; *Wang and Jacob*, 1998; *Prinn et al.*, 1995]. We also considered another CO2-3D simulation driven by an alternative OH distribution with a 5% difference in global mean OH (taken from GEOS-CHEM version 4.33). The resulting shift in the recalculated surface inter-hemispheric gradient of Δy was small (a change of 0.017 ppm, in comparison to the original value of 0.21 ppm). We ascribe this to the relatively low impact of the change in OH on the CO2-3D distribution, and the weak influence of CO2-3D (in comparison to CO2-SURF) on the surface concentrations determining Δy.

[38] *Enting and Mansbridge* [1991] previously addressed the role of the tropospheric CO₂ source from CO oxidation in a simplified zonal mean inversion. They estimated an

increase in Southern Hemisphere sinks of 0.25 Pg C yr^{-1}, and a corresponding decrease in Northern Hemisphere uptake. The regional partitions of the TransCom3 inversion do not permit easy separation of our results into Northern and Southern Hemispheric aggregates (i.e., the tropical regions span the equator). However, separating the northern extratropics (characterized by a decrease in CO_2 uptake) from the tropics and Southern Hemisphere we obtain the following results for (1) the decrease in total (land + ocean) northern uptake and (2) the increase in total tropical and southern sink: 0.21 and 0.20 Pg C year^{-1} (MATCH); 0.20 and 0.21 Pg C yr^{-1} (TM2-LSCE) and 0.18 and 0.17 Pg C yr^{-1} (GISS-Prather). Our results, therefore, appear qualitatively consistent with those of Enting and Mansbridge's earlier study.

[39] We have focused here only on the implications for annual mean inversions following the methodology of the TransCom3 Level 1 analysis. *Rödenbeck et al.* [2003], employing a time-dependent Bayesian technique, solving for monthly fluxes, suggest a much smaller Northern Hemisphere land uptake (0.4–0.5 Pg C yr^{-1}) than the TransCom3 annual mean average (2.2 Pg C yr^{-1}) for the 1992–1996 period. They impute the differences to methodological differences in the inversions. Such results suggest that the magnitude of the chemical pump adjustment may be as or more significant in seasonal time-dependent inversions, and have greater implications for inverse flux estimates on shorter timescales (e.g., monthly). Our calculated chemical pump concentration adjustment (Δy) displays distinct seasonal variation driven by both reduced carbon sources and OH concentrations. The consequent impact on the surface inter-hemispheric difference for Δy (annual mean value of -0.21 ppm) is a range from -0.32 ppm (January) to -0.15 ppm (July). We will explore in future work the implications of this seasonal variability of Δy for inverse CO_2 flux estimates.

References

Altshuller, P. (1991), The production of carbon monoxide by the homogeneous NO$_x$-induced photooxidation of volatile organic compounds in the troposphere, *J. Atmos. Chem.*, *13*, 155–182.

Andres, R. J., G. Marland, I. Fung, and E. Matthews (1996), A 1° × 1° distribution of carbon dioxide emissions from fossil fuel consumption and cement manufacture, 1950–1990, *Global Biogeochem. Cycles*, *10*, 419–429.

Aumont, O., J. C. Orr, P. Monfray, W. Ludwig, P. Amiotte-Suchet, and J. Probst (2001), Riverine-driven interhemispheric transport of carbon, *Global Biogeochem. Cycles*, *15*, 393–405.

Baker, D. (2001), Sources and sinks of atmospheric CO_2 estimated from batch least-squares inversions of CO_2 concentration measurements, Ph.D. thesis, Princeton Univ., Princeton, N. J.

Bergamaschi, P., R. Hein, M. Heimann, and P. J. Crutzen (2000), Inverse modeling of the global CO cycle: 1. Inversion of CO mixing ratios, *J. Geophys. Res.*, *105*, 1909–1927.

Bey, I., D. J. Jacob, R. M. Yantosca, J. A. Logan, B. Field, A. M. Fiore, Q. Li, H. Liu, L. J. Mickley, and M. Schultz (2001), Global modeling of tropospheric chemistry with assimilated meteorology: Model description and evaluation, *J. Geophys. Res.*, *106*, 23,073–23,096.

Bousquet, P., P. Ciais, P. Peylin, M. Ramonet, and P. Monfray (1999), Inverse modeling of annual atmospheric CO_2 sources and sinks: 1. Method and control inversion, *J. Geophys. Res.*, *104*, 26,161–26,178.

Crutzen, P. J. (1994), Global budgets for non-CO_2 greenhouse gases, *Environ. Monit. Assess.*, *31*, 1–15.

Denning, A. S., I. Y. Fung, and D. A. Randall (1995), Latitudinal gradient of atmospheric CO_2 due to seasonal exchange with land biota, *Nature*, *376*, 240–243.

Denning, A. S., J. G. Collatz, C. Zhang, D. A. Randall, J. A. Berry, P. J. Sellers, G. D. Colello, and D. A. Dazlich (1996), Simulations of terrestrial carbon metabolism and atmospheric CO_2 in a general circulation model: Part 1. Surface carbon fluxes, *Tellus, Ser. B*, *48*, 521–542.

Duncan, B. N., R. V. Martin, A. C. Staudt, R. Yevich, and J. A. Logan (2003), Interannual and seasonal variability of biomass burning emissions constrained by satellite observations, *J. Geophys. Res.*, *108*(D2), 4100, doi:10.1029/2002JD002378.

Enting, I. G. (2002), *Inverse Problems in Atmospheric Constituent Transport*, Cambridge Univ. Press, New York.

Enting, I. G., and J. V. Mansbridge (1991), Latitudinal distribution of sources and sinks of CO_2: Results of and inversion study, *Tellus, Ser. B*, *43*, 156–170.

Enting, I. G., C. M. Trudinger, and R. J. Francey (1995), A synthesis inversion of the concentration and $\delta^{13}C$ of atmospheric CO_2, *Tellus, Ser. B*, *47*, 35–52.

Fan, S., M. Gloor, J. Mahlman, S. Pacala, J. Sarmiento, T. Takahashi, and P. Tans (1998), A large terrestrial carbon sink in North America implied by atmospheric and oceanic carbon dioxide data and models, *Science*, *282*, 442–446.

GLOBALVIEW-CO2 (2003), *Cooperative Atmospheric Data Integration Project - Carbon Dioxide* [CD-ROM], Natl. Oceanic and Atmos. Admin. Clim. Monit. and Diagn. Lab., Boulder, Colo. (Available via anonymous FTP to ftp.cmdl.noaa.gov, Path: ccg/co2/GLOBALVIEW)

Guenther, A., et al. (1995), A global model of natural volatile organic compound emissions, *J. Geophys. Res.*, *100*, 8873–8892.

Gurney, K. R., et al. (2002), Towards robust regional estimates of CO_2 sources and sinks using atmospheric transport models, *Nature*, *415*, 626–630.

Gurney, K. R., et al. (2003), TransCom 3 CO_2 inversion intercomparison: 1. Annual mean control results and sensitivity to transport and prior flux information, *Tellus, Ser. B*, *55*, 555–579.

Hansen, J., et al. (1997), Forcings and chaos in interannual to decadal climate change, *J. Geophys. Res.*, *102*, 25,679–25,720.

Heimann, M. (1995), The global atmospheric tracer model TM2, *Tech. Rep. 10*, 51 pp., Dtsch. Klimarechenzentrum, Hamburg, Germany.

Intergovernmental Panel on Climate Change (2001), *Climate Change 2001: The Scientific Basis*, edited by J. T. Houghton et al., Cambridge Univ. Press, New York.

Jacob, D. J., B. D. Field, E. Jin, I. Bey, Q. Li, J. A. Logan, and R. M. Yantosca (2002), Atmospheric budget of acetone, *J. Geophys. Res.*, *107*(D11), 4100, doi:10.1029/2001JD000694.

Kasibhatla, P., A. Arellano, J. A. Logan, P. I. Palmer, and P. Novelli (2002), Top-down estimate of a large source of atmospheric carbon monoxide associated with fuel combustion in Asia, *Geophys. Res. Lett.*, *29*(19), 1900, doi:10.1029/2002GL015581.

Krakauer, N., T. Schneider, J. T. Randerson, and S. C. Olsen (2004), Using generalized cross-validation to select parameters in inversions for regional carbon fluxes, *Geophys. Res. Lett.*, *31*, L19108, doi:10.1029/2004GL020323.

Logan, J. A., M. J. Prather, S. C. Wofsy, and M. B. McElroy (1981), Tropospheric chemistry: A global perspective, *J. Geophys. Res.*, *86*, 7210–7254.

Mahowald, N. M., P. J. Rasch, B. E. Eaton, S. Whittlestone, and R. G. Prinn (1997), Transport of ^{222}Radon to the remote troposphere using the Model of Atmospheric Transport and Chemistry and assimilated winds from ECMWF and the National Center for Environmental Prediction/NCAR, *J. Geophys. Res.*, *102*, 28,139–28,151.

Marland, G., and R. M. Rotty (1984), Carbon dioxide emissions from fossil fuels: A procedure for estimation and results for 1950–1982, *Tellus, Ser. B*, *36*, 232–261.

Marland, G., R. M. Rotty, and N. Treat (1985), CO_2 from fossil fuel burning: Global distribution of emissions, *Tellus, Ser. B*, *37*, 243–258.

Olivier, J. G. J. (2002), On the quality of global emission inventories: Approaches, methodologies, input data and uncertainties, Ph.D thesis, Utrecht Univ., Utrecht, Netherlands.

Petron, G., C. Granier, B. Khattatov, J.-F. Larmarque, V. Yudin, J.-F. Muller, and J. Gille (2002), Inverse modeling of carbon monoxide surface emissions using CMDL network observations, *J. Geophys. Res.*, *107*(D24), 4762, doi:10.1029/2001JD002049.

Peylin, P., D. Baker, J. L. Sarmiento, P. Ciais, and P. Bousquet (2002), Influence of transport uncertainty on annual mean and seasonal inversion of atmospheric CO$_2$ data, *J. Geophys. Res.*, *107*(D19), 4385, doi:10.1029/2001JD000857.

Potter, C. S., J. T. Randerson, C. B. Field, P. A. Matson, P. M. Vitousek, H. A. Mooney, and S. A. Klooster (1993), Terrestrial ecosystem production: A process model based on global satellite and surface data, *Global Biogeochem. Cycles*, *7*, 811–841.

Prather, M. J. (1996), Natural modes and time scales in atmospheric chemistry: Theory, GWPs for CH$_4$ and CO, and runaway growth, *Geophys. Res. Lett.*, *23*, 2597–2600.

Prather, M. J., M. B. McElroy, S. C. Wofsy, G. Russell, and D. Rind (1987), Chemistry of the global troposphere: Fluorocarbons as tracers of air motion, *J. Geophys. Res.*, *92*, 6579–6613.

Prinn, R. G., R. Weiss, B. Miller, J. Huang, F. Alyea, D. Cunnold, D. Hartley, P. Fraser, and P. Simmonds (1995), Atmospheric trends and lifetimes of CH$_3$CCl$_3$ and global OH concentrations, *Science*, *269*, 187–190.

Randerson, J. T., M. V. Thompson, T. J. Conway, I. Y. Fung, and C. B. Field (1997), The contribution of terrestrial sources and sinks to trends in the seasonal cycle of atmospheric carbon dioxide, *Global Biogeochem. Cycles*, *11*, 535–560.

Randerson, J. T., F. S. Chapin, J. W. Harden, J. C. Neff, and M. E. Harmon (2002), Net ecosystem production: A comprehensive measure of net carbon accumulation by ecosystems, *Ecol. Appl.*, *12*(4), 937–947.

Rayner, P. J., I. G. Enting, R. J. Francey, and R. Langenfelds (1999), Reconstructing the recent carbon cycle from atmospheric CO$_2$, d^{13}C, and O$_2$/N$_2$ observations, *Tellus, Ser. B*, *51*, 213–232.

Rödenbeck, C., S. Houweling, M. Gloor, and M. Heimann (2003), Time-dependent atmospheric CO2 inversions based on interannually varying tracer transport, *Tellus, Ser. B*, *55*, 488–497.

Sanderson, M. G. (1996), Biomass of termites and their emissions of methane and carbon-dioxide: A global database, *Global Biogeochem. Cycles*, *10*, 543–557.

Sarmiento, J. L., and E. T. Sundquist (1992), Revised budget for the oceanic uptake of anthropogenic carbon dioxide, *Nature*, *356*, 593–598.

Sellers, P. J., D. A. Randall, G. J. Collatz, J. A. Berry, C. B. Field, D. A. Dazlich, C. Zhang, G. D. Collelo, and L. Bounoua (1996), A revised land surface parameterization (SiB2) for atmospheric GCMs: Part 1. Model formulation, *J. Clim.*, *9*, 676–705.

Spivakovsky, C., et al. (2000), Three-dimensional climatological distribution of tropospheric OH: Update and evaluation, *J. Geophys. Res.*, *105*, 8931–8980.

Suntharalingam, P., D. J. Jacob, P. I. Palmer, J. A. Logan, R. M. Yantosca, Y. Xiao, M. J. Evans, D. Streets, S. A. Vay, and G. Sachse (2004), Improved quantification of Chinese carbon fluxes using CO$_2$/CO correlations in Asian outflow, *J. Geophys. Res.*, *109*, D18S18, doi:10.1029/2003JD004362.

Tans, P. P., I. Y. Fung, and T. Takahashi (1990), Observational constraints on the global atmospheric CO$_2$ budget, *Science*, *247*, 1431–1439.

Walter, B. P., M. Heimann, and E. Matthews (2001), Modeling modern methane emissions from natural wetlands: 1. Model description and results, *J. Geophys. Res.*, *106*, 34,189–34,205.

Wang, Y., and D. J. Jacob (1998), Anthropogenic forcing on tropospheric ozone and OH since preindustrial times, *J. Geophys. Res.*, *103*, 31,123–31,135.

Wang, J. S., J. A. Logan, M. B. McElroy, B. N. Duncan, I. A. Megretskaia, and R. M. Yantosca (2004), A 3-D model analysis of the slowdown and interannual variability in the methane growth rate from 1988 to 1997, *Global Biogeochem. Cycles*, *18*, GB3011, doi:10.1029/2003GB002180.

World Meteorological Organization (1999), Scientific assessment of ozone depletion: 1998, *Rep. 44*, Global Ozone Res. Monit. Proj., Geneva.

Yevich, R., and J. A. Logan (2003), An assessment of biofuel use and burning of agricultural waste in the developing world, *Global Biogeochem. Cycles*, *17*(4), 1095, doi:10.1029/2002GB001952.
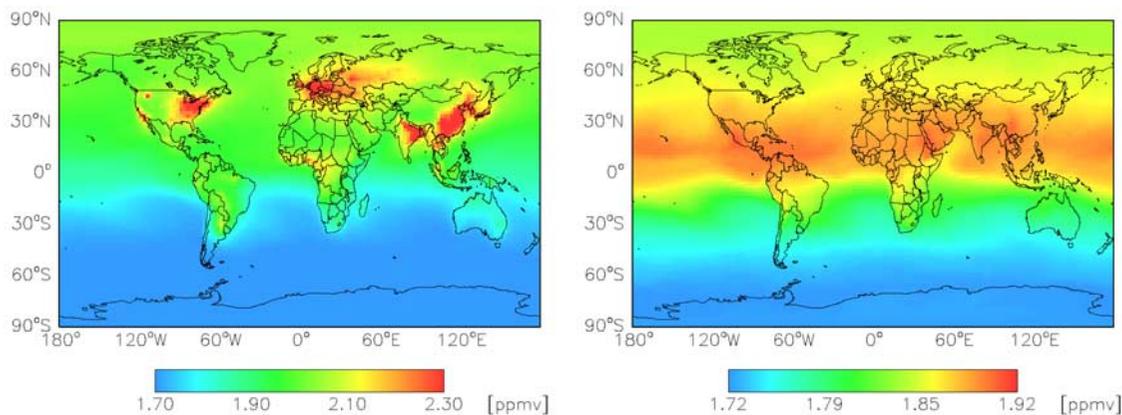

D. J. Jacob, J. A. Logan, and P. Suntharalingam, Division of Engineering and Applied Sciences, Harvard University, Pierce Hall, 29 Oxford Street, Cambridge, MA 02138, USA. (djj@io.harvard.edu; jal@io.harvard.edu; pns@io.harvard.edu)

N. Krakauer, Division of Geological and Planetary Sciences, California Institute of Technology, MC 100-23, Pasadena, CA 91125, USA. (niryk@caltech.edu)
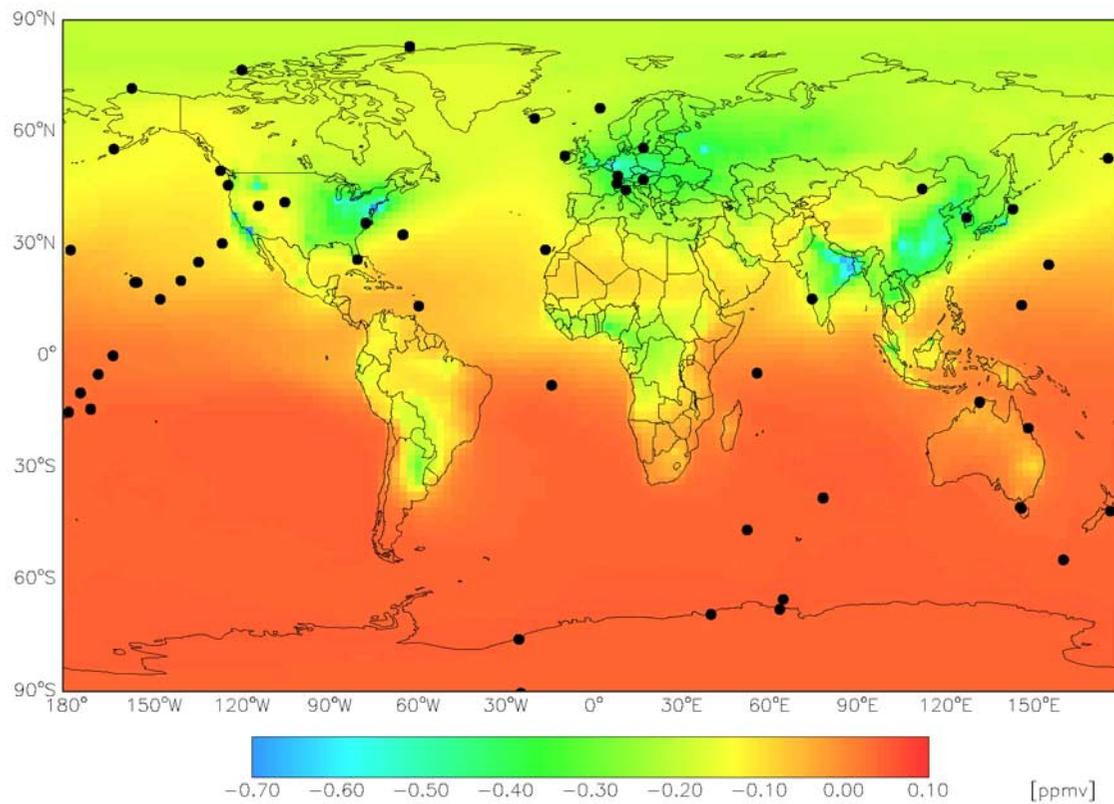
J. T. Randerson, Department of Earth System Science, University of California, 3212 Croul Hall, Irvine, CA 92697, USA. (jranders@uci.edu)
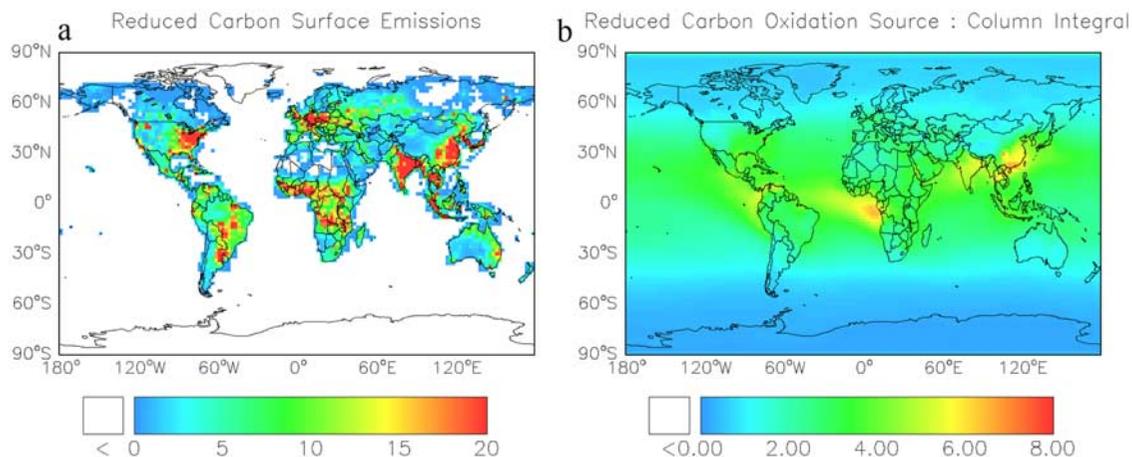
Figure 1. Global distributions of the CO$_2$ source from (a) surface emissions of these reduced carbon trace gases (the fluxes specified in the CO2-SURF simulation, left panel); and (b) the oxidation of reduced carbon trace gases (the column integrals of the CO$_2$ fluxes from the CO2-3D simulation, right panel). The total carbon source is the same in both distributions (1.1 PgCyr^{-1}). Units are gC m^{-2} yr^{-1}. The two panels have different color scales to highlight spatial features.

Figure 3. Surface CO$_2$ concentration distributions from (left) the CO2-SURF simulation (for Δy_{surf}) and (right) the CO2-3D simulation (for Δy_{ox}). Values shown are the annual mean concentration in the fourth simulation year, and following subtraction of the initial condition (370 ppm). The two panels have different color scales to highlight spatial features.

Figure 4. Spatial distribution of the chemical pump concentration adjustment $\Delta\mathbf{y}$ at the surface (annual mean). This distribution represents the difference between the left and right panels of Figure 3 ($\Delta\mathbf{y_{ox}} - \Delta\mathbf{y_{surf}}$). Units are ppm. The black circles represent the GLOBALVIEW-CO2 stations used in the inversion analysis of *Gurney et al.* [2002].